Low-Power LC-VCO using integrated MEMS passives

Vivek Kumar Saraf*, Deepa Ramachandran*, Altug Oz*, Gary K. Fedder*† and Tamal Mukherjee*

*Department of Electrical and Computer Engineering and †The Robotics Institute,
Carnegie Mellon University, 5000 Forbes Ave., Pittsburgh, PA 15213-3890, USA.

Abstract — **Low power RF operation is often limited by the poor quality factor of the passives available in silicon-based processes. This paper reports on a LC-tank VCO incorporating micromachined inductors and capacitors for low power operation without sacrificing performance. Only 2.75 mW of power is needed to achieve -122 dBc/Hz phase noise at 1 MHz from a 2.84 GHz carrier.**

Index Terms — **voltage controlled oscillators, phase noise, micromachining, inductor, varactor, Q factor.**

I. Introduction

Portable mobile communications systems inevitably require low power operation. The power needed to achieve desired RF performance is dictated by process technology, in particular the Q-factor of the passives. Silicon-based passives inherently suffer from low Q-factors. Recent processing enhancements to improve Q include thicker metallizations and thicker dielectric spacer layers as well as higher substrate resistivity. Post-foundry micromachining enables integration of RF electronics with RF MEMS suspended inductors [1] and MEMS capacitors [2]. It further enhances the Q factor of the MEMS passives needed for the design of low power oscillators with low phase noise. Although MEMS inductors were integrated with electronics about 10 years ago [3], recent RF MEMS inductors [4] and capacitors [5] have used customized processing, preventing integration. The oscillators in this paper use a foundry fabricated interconnect stack for the RF passives, enabling monolithic integration with electronics, and eliminating losses arising from bonding custom fabricated RF MEMS passive chips to electronics ICs.

II. Phase Noise In A Differential LC VCO

The cross-coupled differential configuration is used for the VCO as shown in Fig 1. The LC tank consists of micromachined inductor, micromachined capacitor (for digital tuning) and varactor diode (for analog tuning). The current source shown in the figure is implemented by a bipolar current mirror, which mirrors current from an off-chip source so that the bias current can be measured accurately. The reduced *1/f* corner frequency of the bipolar tail current source ensures that the low frequency noise upconversion occurring due to circuit non-linearities (varactor etc.) is low. The expression for phase noise calculation at an offset f_m from the carrier frequency f_o can be traced from the classical Leeson's model [6]

$$PN(f_m) = \frac{2 \cdot k \cdot T \cdot F \cdot R_p}{A_o^2}\left(\frac{f_o}{2 \cdot Q \cdot f_m}\right)^2\left(1 + \frac{\Delta f_{1/f^3}}{f_m}\right)^2 \qquad (1)$$

where k is Boltzmann's constant, T is the absolute temperature, A_o is the amplitude of oscillation, Q is the resonator loaded quality factor, R_p is the parallel resistance used to model the losses in the resonator, $\Delta f_{1/f^3}$ is the $1/f^3$ corner frequency in the phase noise spectrum and F is the excess noise factor. It can be seen from (1) that phase noise drops by the square of A_o and tank Q. A disadvantage of using a CMOS cross-coupled pair is that it is not possible for the swing to exceed the supply voltage. The bipolar implementation of the cross-coupled pair allows swings higher than the rails. This is aided by DC-decoupling the base and collector of the cross-coupled pair with a capacitive divider as shown in Fig 1, preventing forward bias of the C-B junction and hence allowing greater swing on the collectors.

While increasing the swing does improve the phase noise, it does so at the cost of increased power consumption, since the oscillation amplitude is simply the product of R_p with current flowing across the tank. Low power implementation is best served by increasing the Q as much

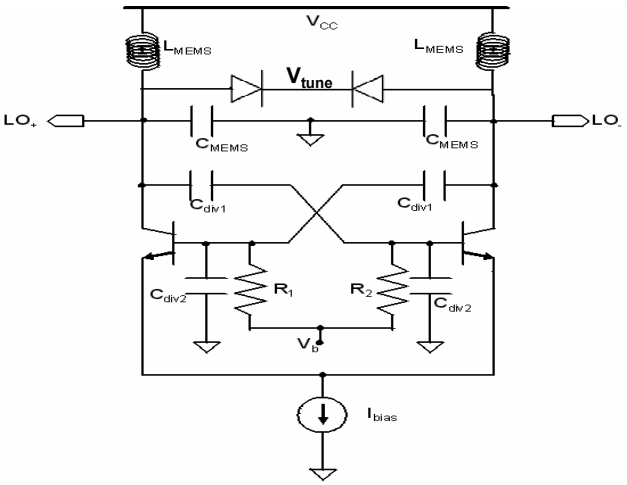

Fig. 1. VCO schematic with MEMS enhanced passives

as possible. This also indirectly increases A_o by increasing R_p (since R_p models the tank loss, which is now reduced), and hence reduces phase noise.

III. MEMS-enhanced Integrated Passives

For silicon-based technologies, the challenge in increasing tank Q is the limited Q_{max} of the on-chip inductor. Differential inductors are used in this paper as they have improved Q over their single-ended counterparts [7]. Micromachining further enhances inductor Q_{max} [1].

The micromachining process [8] removes the dielectric between inductor turns as well as ~30 μm of silicon under the RF passives, which in turn reduces coupling to the lossy Si substrate. A lumped parameter schematic model for the inductor from the foundry design kit [9] and a full wave method of moments solver [10] were used to design the inductor. These simulations indicate that, for the 6.25 nH differential inductor used in this paper, a 2X improvement in Q_{max} occurs due to micromachining. Also, at the oscillation frequency of 2.8 GHz, micromachining increases the Q of the 6.25 nH from 6 to 16 as shown in Fig 2. This graph clearly shows the benefit of micromachining. The remaining curves (with the center-tap floating for single-ended simulation) are included to help compare with the measured results to be described in Section IV.

A small varactor diode is used in parallel with a fixed capacitance in the VCO tank (Fig 1) to allow for tuning around the desired center frequency. To achieve the same tuning range from a smaller varactor, as well as to minimize losses through the substrate we desire to minimize the parasitic capacitance from the fixed capacitor. The ability to remove the silicon under the micromachined capacitor is used to reduce this parasitic capacitance.

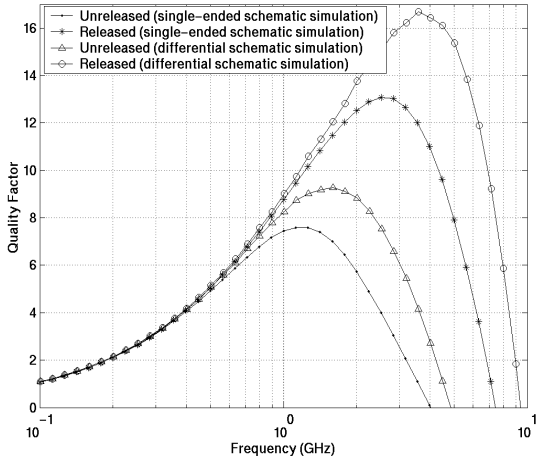

Fig. 2. Quality factor vs. frequency for a 6.25-nH inductor.

The micromachined capacitor (shown in Fig 3) is composed of interdigitated beams with multiple electrodes. The dielectric between the interdigitated beams is removed to access the silicon surface so as to remove the lossy silicon from under the capacitor. This capacitor can also be used as a varactor, by changing the gaps between these beams using the electrothermal actuators. In this paper we only use the low parasitic nature of this capacitance, with the latch to hold the capacitor at its minimum capacitance configuration [11].

IV. Measurement Results

An LC-tank oscillator implementing the schematic of Fig 1 was fabricated in the Jazz SiGe60 (0.35μm) process. Test structures of the passive components were included to measure the enhanced Q arising from micromachining. In this section we describe the enhancements arising from micromachining for both the passive devices and the VCO.

A. Inductor Characterization Results

Fig 4 shows quality factor vs. frequency for a test 2-nH differential layout but with center-tap floating. The plots have been made after de-embedding the pad and interconnect parasitics by the commonly used Y-Parameter method. There are 2 sets of curves in this graph — one set is for the unreleased case (with the inductor as is after foundry BiCMOS processing) and the second set is for the released case (after the post-foundry micromachining). Within each set, there are 3 curves — measured, lumped parameter schematic model [9] and a fast method of moments solver [10]. From the graph, it can be seen that the 3 plots are in excellent agreement for the unreleased case. For the released case, the Ultrasyn solver matches the measured data until 1 GHz, and is a little optimistic beyond 1 GHz. The schematic model also matches the measured data up to 3 GHz, and underestimates Q at frequencies

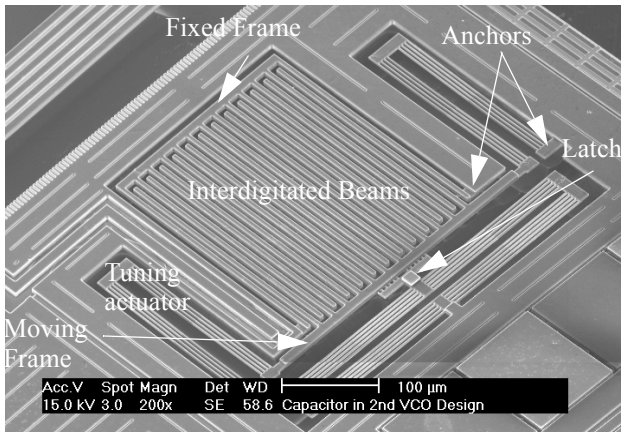

Fig. 3. SEM of MEMS Capacitor

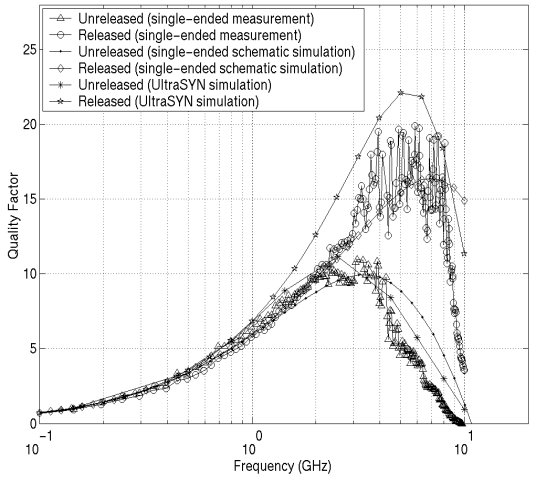

Fig. 4. Quality factor vs. frequency for a 2-nH inductor

beyond 3 GHz. Due to space considerations, the chip did not include a 6.5 nH inductor used in the VCO. However, as the schematic model underestimates the measured Q for the 2 nH case, we only present schematic model simulations of the 6.5 nH inductor in Fig 2 to describe the potential Q enhancement possible through micromachining.

B. Capacitor Characterization Results

For low power operation the capacitor should not degrade the tank Q. The dominant resistive loss in the MEMS capacitor is the series resistance of the interconnect in the actuator (on the bottom-left and top-right in Fig 3). The calculated value of the series resistance for the MEMS capacitor is about 20 Ω, resulting in a calculated Q of 20 at 2.8 GHz (Fig 5). The measured Q for the capacitor test structure, also shown in Fig 5, is 30 at 2.8 GHz, due to conservative models used in calculation. As this paper focuses on low power operation, the use of the lateral actuators to change the gap between the interdigitated beams in the capacitor was not exercised.

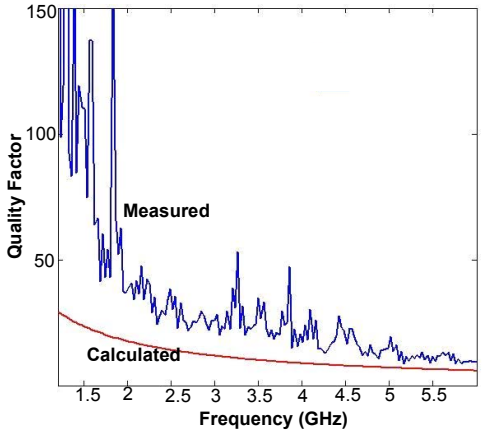

Fig. 5. Q-factor characteristics of MEMS capacitors.

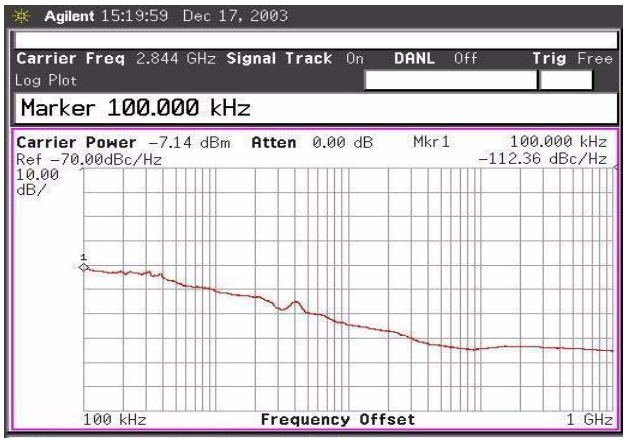

Fig. 6. Phase Noise Plot of VCO

C. VCO Results

The fabricated VCO had a center frequency of 2.84 GHz, with a tuning range of 150 MHz from the varactor used (see Fig 1). As described in Section II, the tank Q strongly affects the phase noise performance. Here we describe two ways through which the high tank Q improved the VCO performance. The improvement of Q due to micromachining can be demonstrated from the minimum bias current required to start oscillations. Only 125 μA was needed for the oscillator after release, compared to 520 μA for the same oscillator before micromachining. The improvement of tank Q can also be demonstrated by comparing measured phase noise for the same bias current. Fig 6 shows the measured phase noise spectrum, obtained on an Agilent E4440A Spectrum Analyzer using Phase Noise Personality. Oscillator performance for the same bias current of 1.1 mA is reported in Table 1, showing that micromachining results in a phase noise improvement of 21 dBc/Hz.

V. Comparison with VCOs in Literature

The previous section focused on the enhancements arising from micromachining. Here we compare the VCO with other previously published VCOs employing micromachined passives. These results are summarized in Table 2. The Figure of Merit (FoM) [12] is used to compare the results,

TABLE 1.
IMPACT OF MICROMACHINING ON OSCILLATOR PERFORMANCE

	f_o (GHz)	PN @ 1 MHz (dBc/Hz)	P_{diss} (mW)	FoM (dB)
Before release	1.64	-106	2.75	166
After release	2.84	-122	2.75	187

$$FoM = 10log\left(\left(\frac{f_o}{\Delta f}\right)^2 \times \frac{1}{L\{\Delta f\}P}\right) \quad (2)$$

where f_o is the carrier frequency, Δf is the offset from f_o, $L\{\Delta f\}$ is the phase noise at that offset and P is the power consumed in the core in mW. A common design procedure to minimize phase noise is to choose a small value of L allowing a bigger value of C, to lower the kT/C noise [15]. This however leads to a higher power consumption, since more current is needed for the same oscillation amplitude for a bigger C, as can been seen from Table 2. The proposed scheme not only makes use of a bigger L to decrease power consumption but also exploits the high Q of the micromachined inductor to offset the phase noise degradation due to a small C, allowing comparable phase noise performance.

As shown in Fig. 2, micromachining starts improving Q for frequencies greater than 1 GHz. With the trend to higher frequency RF communications, there is abundant scope for exploiting this in VCO designs, particularly since the quality factors of conventionally implemented passives is limited by both substrate loss and self-resonance at these frequencies. This FoM achieved in this design outperforms all previously published VCOs using stock CMOS processes with frequencies greater than 2 GHz, due to the magnitude decrease in power consumed.

VI. Conclusion

In summary, post-foundry micromachining of integrated RF passives was used to reduce loss. Integration with a cross-coupled pair led to low power oscillator operation. The resulting FoM of 187 is better than all previous VCOs based on micromachining. The design uses a magnitude of less power than other VCOs at similar operating frequencies. The use of micromachining is particularly promising for low power operation at high frequencies as its enhancement of inductor Q increases with frequency.

Table 2.
LC Oscillator Comparison

	This Work	Ref [13]	Ref [14]
f_o (GHz)	2.84	2.4	2.6
PN (dBc/Hz)	-122	-122	-127
P_{diss} (mW)	2.75	13.5	15
FoM (dB)	187	178	184
L (nH)	6.25	2.8	1.8
C (pF)	0.5	1.4	2
Idea	MEMS L & C	MEMS C	MEMS L

Acknowledgement

This research effort was supported by the MARCO/ DARPA Focus Center on Circuits and Systems Solutions (C2S2) under award MDA972-02-1-0004 and by DARPA NMASP program under award DAAB07-02-C-K001 and DARPA NeoCAD program under award F33615-01-2-1970. The authors would also like to thank Neolinear for access and support to the fast UltraSYN solver.

References

[1] H. Lakdawala, X. Zhu, H. Luo, S. Santhanam, L. R. Carley, G. K. Fedder, "Micromachined High-Q Inductors in 0.18 μm Cu Interconnect Low-K CMOS," *JSSC*, SC-37(3), Mar. 2002, pp. 394-403.

[2] A. Oz, G. K. Fedder, "CMOS-Compatible RF-MEMS Tunable Capacitors," *2003 IEEE Int. RFIC Symp.*, pp. 611-614.

[3] J.Y.-C. Chang, A.A. Abidi, M. Gaitan, "Large suspended inductors on silicon and their use in a 2-μm CMOS RF amplifier," *IEEE Elec. Dev. Lett.*, Vol. 14 no. 5, pp. 246-248.

[4] H. Jiang, J.-L.A.Yeh, Y. Wang, and N. Tien, "Electromagnetically shielded high-Q CMOS-compatible copper inductors," *ISSCC Dig. Tech. Papers*, pp. 330-331, 2000.

[5] A.Dec, K. Suyama, "A 1.9-GHz CMOS VCO with micromachined electromechanically tunable capacitors, *JSSC*, SC-35(8), Aug. 2000, pp. 1231-1237.

[6] D. B. Leeson, "A Simple Model of Feedback Oscillator Noise Spectrum," *Proc. IEEE*, 54(2), pp. 329-330, 1966.

[7] W. B. Kuhn, A. Elshabini-Riad, F. W. Stephenson, "Centre-tapped spiral inductors for monolithic bandpass filters," *Electronic Letters*, vol. 31, no.8, 13 April 1995, p.625-6.

[8] G. K. Fedder, S. Santhanam, M. L. Reed, S. C. Eagle, D. F. Guillou, M. S.-C. Lu, and L. R. Carley, "Laminated High-Aspect-Ratio Microstructures In A Conventional CMOS Process," *Sensors & Actuators*, pp. 103-110, March 1997.

[9] Jazz Semiconductor, "SiGe60 (sbc35) Design Manual," *http://www.jazzsemi.com*, 2003.

[10] F. Ling V. Okhmatovski, W. Harris, S. McCraken and A. Dengi, "Large-Scale Broadband Parasitic Extraction for Fast Layout Verification of 3D RF and Mixed-Signal On-Chip Structures," in *IMS 2004*, Forth Worth TX, June 6-11, 2004.

[11] D. Ramachandran, A. Oz, V. K. Saraf, G. K. Fedder and T. Mukherjee, "MEMS-enabled Reconfigurable VCO and RF Filter," *RFIC 2004*, Fort Worth, TX, June 6-8, 2004.

[12] P. Kinget, "Integrated GHz voltage controlled oscillators," in *Analog Circuit Design: (X)DSL and Other Communication Systems; RF MOST Models; Integrated Filters and Oscillators*, W. Sansen, J. Huijsing, and R. van de Plassche, eds. Boston, MA: Kluwer, 1999, pp. 353-381.

[13] A.Dec, K. Suyama, "Microwave MEMS-based voltage controlled oscillators,," *Trans. MTT*, MTT-48(11), Nov. 2000, pp. 1943-1949

[14] E.-C. Park, Y.-S. Choi, J.-B. Yoon, S. Hong and E. Yoon, "Fully integrated low phase-noise VCOs with on-chip MEMS inductors," *Trans. MTT*, MTT-51(1), Jan. 2003, pp. 289-296.

[15] D.Ham, A. Hajimiri, "Concepts and methods in optimization of integrated LC VCOs, *JSSC*, SC-36(6), June 2001, pp. 896-909.